Available online at www.sciencedirect.com
ScienceDirect
International Journal of Heat and Fluid Flow 29 (2008) 774–782
International Journal of HEAT AND FLUID FLOW
www.elsevier.com/locate/ijhff

The effects of swell on turbulence over wavy walls

Ryoichi Kurose, Takanori Imashiro, Satoru Komori *

Department of Mechanical Engineering and Science, Advanced Research Institute of Fluid Science and Engineering, Kyoto University, Yoshida-honmachi, Sakyo-ku, Kyoto 606-8501, Japan

Received 26 October 2007; received in revised form 23 January 2008; accepted 24 January 2008
Available online 14 March 2008

Abstract

Three-dimensional direct numerical simulations (DNS) are applied to the turbulent air boundary layer over a wavy wall, which imitates the air–water interface consisting of both wind waves and swells, and the effects of the swells with various directions on the turbulence structure and drag over/on the wavy wall are investigated. The results show that parallel swell with the same direction as the wind increases the turbulence intensity and the Reynolds stress over the wavy wall. The swell also increases the pressure drag and decreases the friction drag on the wavy wall, and consequently increases the total drag because of remarkable increase of pressure drag. As the inclination angle of the swell against the wind increases from parallel to perpendicular, the swell effect on the drag becomes weak and finally vanishes. The reduction of friction drag due to swell supports our previous measurements that show reduction of the mass transfer velocity across the wind-driven wavy air–water interface due to the parallel swell.

Keywords: Turbulent flow; Boundary layer; Wavy wall; DNS; Swell

1. Introduction

Global warming, which has become one of the most serious environmental problems in recent decades, is known to be caused by emissions of greenhouse gasses such as carbon dioxide (CO_2) and methane (CH_4). In order to predict the increase of atmospheric temperature, it is of great importance to precisely estimate the global carbon cycle. One of the important issues is to precisely predict mass transfer velocity of greenhouse gases across the air–sea interface between atmosphere and oceans. In GCMs (general circulation models) for climate change simulations, the mass transfer velocity has been correlated with only wind speed observed over oceans (e.g. Wanninkhof, 1992). However, the relations between the mass transfer velocity and the wind speed are greatly scattered. One of the reasons why field measurements of mass transfer velocity are so scattered is that the air–sea mass transfer is affected by other factors besides wind speed. Generally, there exist two types of waves in oceans: wind waves generated by only wind shear acting on the air–sea interface, and swells propagated from afar with low frequency. Our previous measurements in a wind wave tank (Komori et al., 1993a; Tanno and Komori, 2004) showed that the swell decreases the mass transfer velocity across the air–water interface in a limited case where the phase velocities of the swell and wind wave are slower than the wind velocity. However, it has not been clarified why the swell reduces the mass transfer velocity. To explicitly understand the swell effect, the drag force acting on the interface should be carefully investigated, since mass transfer is promoted by turbulent motions (surface-renewal eddies) beneath the air–water interface, and the surface-renewal eddies are produced mainly by drag on the interface (Komori et al., 1989, 1993a,b).

Three-dimensional direct numerical simulation (DNS) and large-eddy simulation (LES), which solve air–water two phase flows, are useful tools for investigating the turbulence structure in both air and water flows, and also the drag on the interface (Lakehal et al., 2003; Fulgosi et al., 2003; Magnaudet and Calmet, 2006). However, these

* Corresponding author.
E-mail address: komori@mech.kyoto-u.ac.jp (S. Komori).

0142-727X/$ - see front matter © 2008 Elsevier Inc. All rights reserved.
doi:10.1016/j.ijheatfluidflow.2008.01.014

Notation

A	vertical projected area of wall
$\boldsymbol{e}_l$	wall tangential unit vector
$\boldsymbol{e}_n$	wall normal unit vector
$\boldsymbol{e}_x$	streamwise unit vector
$D_{F,f}$	friction drags on flat wall
$D_{F,w}$	friction drags on wavy wall
$D_{P,w}$	pressure drags on wavy wall
D_T	total of all drags ($=D_{F,f}+D_{P,w}+D_{F,w}$)
$D_{T,w}$	total of drags on wavy wall ($=D_{P,w}+D_{F,w}$)
$D_{F,case\,2}$	friction drags on wavy wall in case 2
P	pressure
p_w	pressure on wall
p_0	standard pressure on wavy wall
Re	Reynolds number based on half height of computational domain and streamwise maximum mean velocity, $Re=\frac{U_{max}\cdot\delta}{\nu}$
t	time
U_i	instantaneous velocity component in i direction (U,V,W)
u_*	friction velocity on wavy wall
u_{rms}, v_{rms}, w_{rms}	root mean square of U_i
x_i	coordinates in i direction (x,y,z)
x,y,z	streamwise, spanwise and vertical coordinates
z'	distance from wavy wall

Greeks

α	a constant to control the convergence of grid (=3.1)
δ	half height of the computational domain
θ	angle between wind and swell
λ	wave length of wind wave
ρ	density
τ_w	shear stress on wall
ν	kinematic viscosity
ς_i	coordinate of uniform grid

Superscripts

$\bar{()}$	ensemble average
$()^+$	normalization by wall variables (u_*,ν)

DNS and LES require huge computation time and big computational domain especially when wind waves and swells co-exist (referred to as swell wind wave, hereafter). To save computation time and to preserve the wide computational domain for the swell wind wave, it is practical to apply the DNS or LES to only air flow over a wavy rigid wall with similar shape to the air–water interface of the swell wind wave.

Turbulent flows over wavy rigid walls have been examined in many studies (e.g. Günther and von Rohr, 2003; Hudson et al., 1996; Krettenauer and Schumann, 1992; Poggi et al., 2003). Zilker et al. (1977) experimentally investigated the influence of the wave amplitude. Komori (1996) studied the turbulence structure over a three-dimensional wavy wall by DNS. Angelis et al. (1997) investigated the effect of wavelength on turbulence structure over a wavy wall by DNS. Nakagawa and Hanratty (2001) measured the turbulence structure over the wavy wall using PIV (particle image velocimetry). On the other hand, Sullivan et al. (2000, 2002) investigated the turbulence structure over the travelling wavy wall which emulates the real moving wind wave, and Belcher and Hunt (1998) reviewed the researches about the turbulent flow over the wavy terrain from theoretical aspects. However, these researches have not discussed the swell effect. Recently, Nakayama and Sakio (2003) applied the DNS to a turbulent flow over a complex wavy wall, which consisted of two types of waves with different wavelengths. In their studies, however, the drag on the wavy wall was not well investigated.

The purpose of this study is, therefore, to clarify the swell effects on the turbulence structure and drag (pressure and friction drag) on the air–water interface consisting of both wind waves and swells by applying a three-dimensional DNS to turbulent air flow over the wavy rigid wall with similar shape to the interface. Six types of wavy walls with shapes corresponding to pure wind wave and swell wind waves with five different angles to the wind direction are used here.

2. Direct numerical simulation

The three-dimensional continuity and Navier–Stokes equations for incompressible fluids:

$$\frac{\partial U_i}{\partial x_i}=0, \tag{1}$$

$$\frac{\partial U_i}{\partial t}+U_j\frac{\partial U_i}{\partial x_j}=-\frac{1}{\rho}\frac{\partial P}{\partial x_i}+\nu\frac{\partial^2 U_i}{\partial x_j\partial x_j}, \tag{2}$$

were directly solved using the finite difference method (Marker and Cell method). The details of the present numerical method and the accuracy are described in our previous paper (Komori et al., 1993b).

The computational domains and their details are shown in Fig. 1 and Table 1. Turbulent air flows over the six wavy walls: pure wind wave (case 1) and swell wind waves with five inclination angles with respect to the wind direction (cases 2–6), were computed. In Table 1, λ ($=1.0\times10^{-2}$ m) is the wavelength of the wind wave. The inclination angles of the swell to the wind direction, θ, in cases 2–6 were 0°, 27°, 48°, 70° and 90°, respectively. The swells with wind waves in cases 2 and 6 are referred to as "parallel-swell wind wave" and "perpendicular-swell wind wave", respectively, and swell wind waves in cases 3–5 are referred

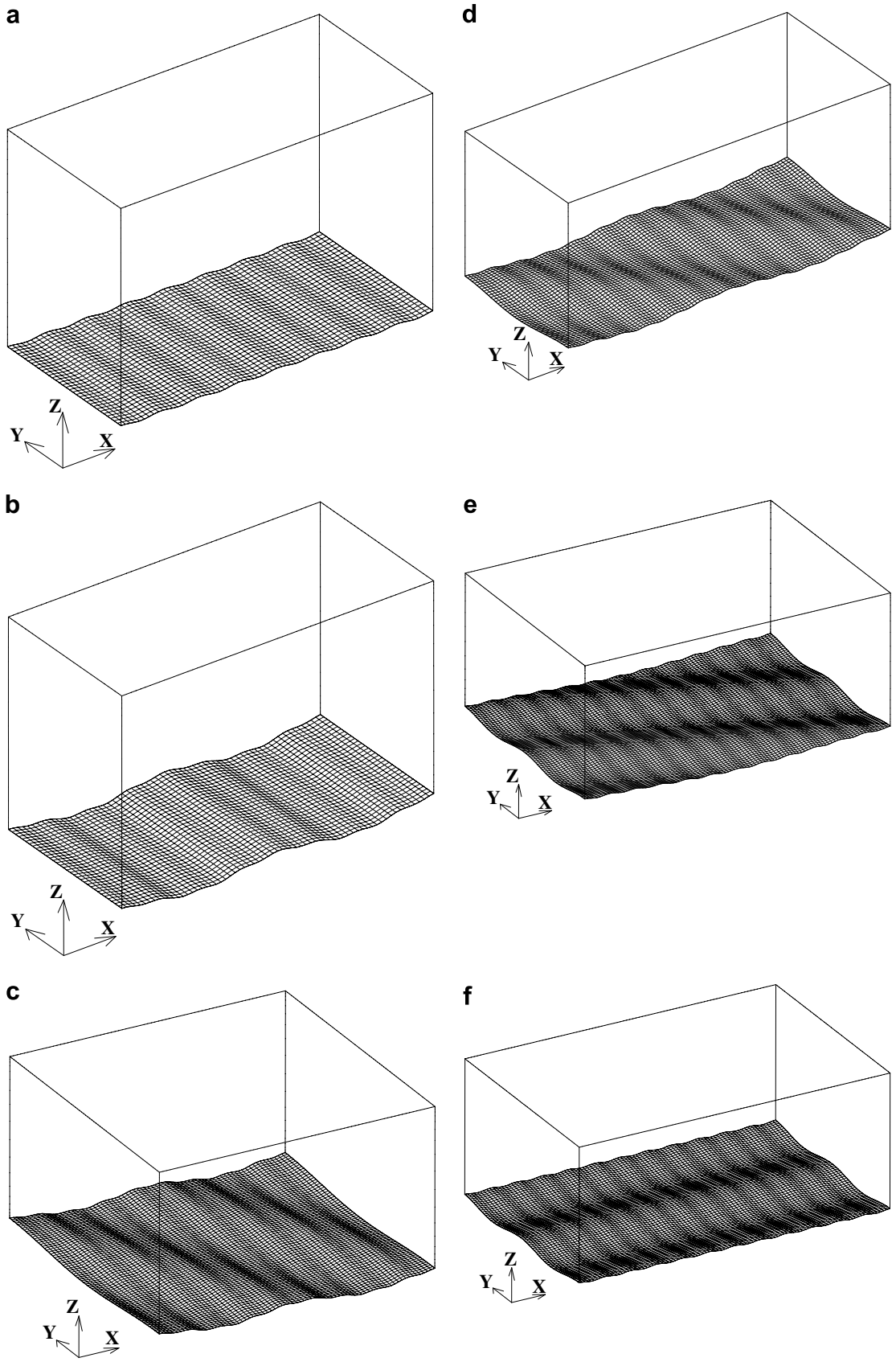

Fig. 1. Shapes of wavy walls: (a) case 1: pure wind wave; (b) case 2: parallel-swell wind wave (0° oblique-swell); (c) case 3: 27° oblique-swell wind wave; (d) case 4: 48° oblique-swell wind wave; (e) case 5: 70° oblique-swell wind wave; (f) case 6: perpendicular-swell wind wave (90° oblique-swell).

Table 1
Computational domains

Case	Wave type	Size ($x \times y \times z$)	Grid points
Case 1	Pure wind wave	$8\lambda \times 4\lambda \times 5.2\lambda$	$200 \times 100 \times 200$
Case 2	Parallel-swell wind wave (0° oblique-swell wind wave)	$8\lambda \times 4\lambda \times 5.2\lambda$	$200 \times 100 \times 200$
Case 3	27° oblique-swell wind wave	$9\lambda \times \frac{36\sqrt{17}}{17}\lambda \times 5.2\lambda$	$230 \times 220 \times 200$
Case 4	48° oblique-swell wind wave	$12\lambda \times \frac{12\sqrt{5}}{5}\lambda \times 5.2\lambda$	$300 \times 134 \times 200$
Case 5	70° oblique-swell wind wave	$12\lambda \times 6\sqrt{2}\lambda \times 5.2\lambda$	$300 \times 220 \times 200$
Case 6	Perpendicular-swell wind wave (90° oblique-swell wind wave)	$12\lambda \times 8\lambda \times 5.2\lambda$	$300 \times 200 \times 200$

to as "oblique-swell wind wave", hereinafter. The sizes of the domains and θ were defined to accomplish both the streamwise and spanwise periodic conditions for the wavy walls. The wind waves and swells were approximated as sinusoidal waves and the shapes of the swell wind waves were acquired as the sum of their sinusoidal components. The wave heights of the wind waves and swells were 0.055λ and 0.225λ and their wavelengths were λ and 4λ, respectively. Periodic boundary conditions were applied in the streamwise and spanwise directions. Non-slip boundary conditions were applied to both the upper flat wall and lower wavy wall. The computational grids are converged to the walls by using the function of $z_i = 1 - \frac{\tanh(\alpha\varsigma_i)}{\tanh(\alpha)}$. Here, ς_i is the coordinate of uniform grid ($0 \leqslant \varsigma_i \leqslant 1$) and α (=3.1) is a constant to control the convergence. The wind was driven in the x direction over the wavy walls by the constant mean pressure gradient, $\frac{\partial p}{\partial x}$ (=5.3 N/m^3), which was the same value in all cases. The Reynolds number, $Re = \frac{U_{\max}\cdot\delta}{\nu}$, defined by the maximum streamwise velocity, $U_{\max}$, the half height of the computational domain, δ (=2.6λ), and the kinematic viscosity, ν, varied from 9800 to 11,800.

3. Results and discussion

3.1. Turbulence structure over wavy walls

Fig. 2 shows the distributions of instantaneous streamwise velocity on the x–z plane in cases 1, 2 and 4. A developed turbulent boundary layer is observed over the wavy walls. In cases 2 and 4, the streamwise velocity becomes negative on the leeward side of the swells. This is because a reverse flow is generated by flow separation on this side. The reverse flow is stronger in case 2 than in case 4.

The distribution of instantaneous spanwise velocity on the y–z plane in case 4 is shown in Fig. 3. The spanwise velocity takes a remarkable negative value on the windward side of the oblique swell (see region **A**). This is because the oblique swell guides the flow near the wavy wall. This can be understood from the instantaneous velocity vectors near the wavy wall in case 4 (see Fig. 4). The velocity takes a negative spanwise value near the trough on the windward side of the oblique swell and weakly positive value on the crest of the swell.

Fig. 5 shows the distributions of mean streamwise, spanwise and vertical velocities in case 4. These values are obtained by taking the time- and space- averages in the streamwise and spanwise directions in the region higher than the top of the wavy walls. Hereafter, other turbulence statistics in the following figures will be calculated in the same way. Mean streamwise velocity is small near the upper and lower walls as in general channel flows. It is also found that the velocity near the lower wavy wall is smaller than that near the upper flat wall, and the location where the velocity indicates the maximum value is higher than the centre of the domain. These properties of the flow occur because the drag on the lower wavy wall is larger than that on the upper flat wall, as will be mentioned later. The vertical velocity is zero in the whole region, but the spanwise velocity takes a small negative value. This is consistent with Figs. 3 and 4.

Fig. 6 shows the distributions of mean streamwise velocity in cases 1, 2 and 4. These values are non-dimensionalized by the friction velocity, u_*, calculated from the total drag on the wavy walls, $D_{T,w}$, which will be mentioned later. In all cases, the distributions have a log-law region. Since the forced pressure gradients are the same value but the drags on the wavy walls are different, their maximum velocities are different.

The distributions of turbulence intensities and the Reynolds stress over the wavy walls in cases 1, 2 and 4 are shown in Figs. 7 and 8, respectively. These values are non-dimensionalized by u_*. The turbulence intensities in cases 2 and 4 are found to be generally stronger than those in case 1. However, the streamwise component of that near the wavy wall in cases 2 and 4 is smaller than that in case 1. This is because the wall's crest in cases 2 and 4 is higher than in case 1. The Reynolds stress in cases 2 and 4 is also found to be stronger than those in case 1. These indicate that turbulence is promoted by the parallel and oblique swells. This also suggests that both the parallel- and oblique- swells tend to promote turbulence over the wind-driven air–water interface consisting of swells and wind waves.

3.2. Pressure and friction drag on wavy walls

The drag consists of pressure drag, D_P, and friction drag, D_F. The pressure and friction drags are obtained by integrating pressure and shear stress on the wavy walls as

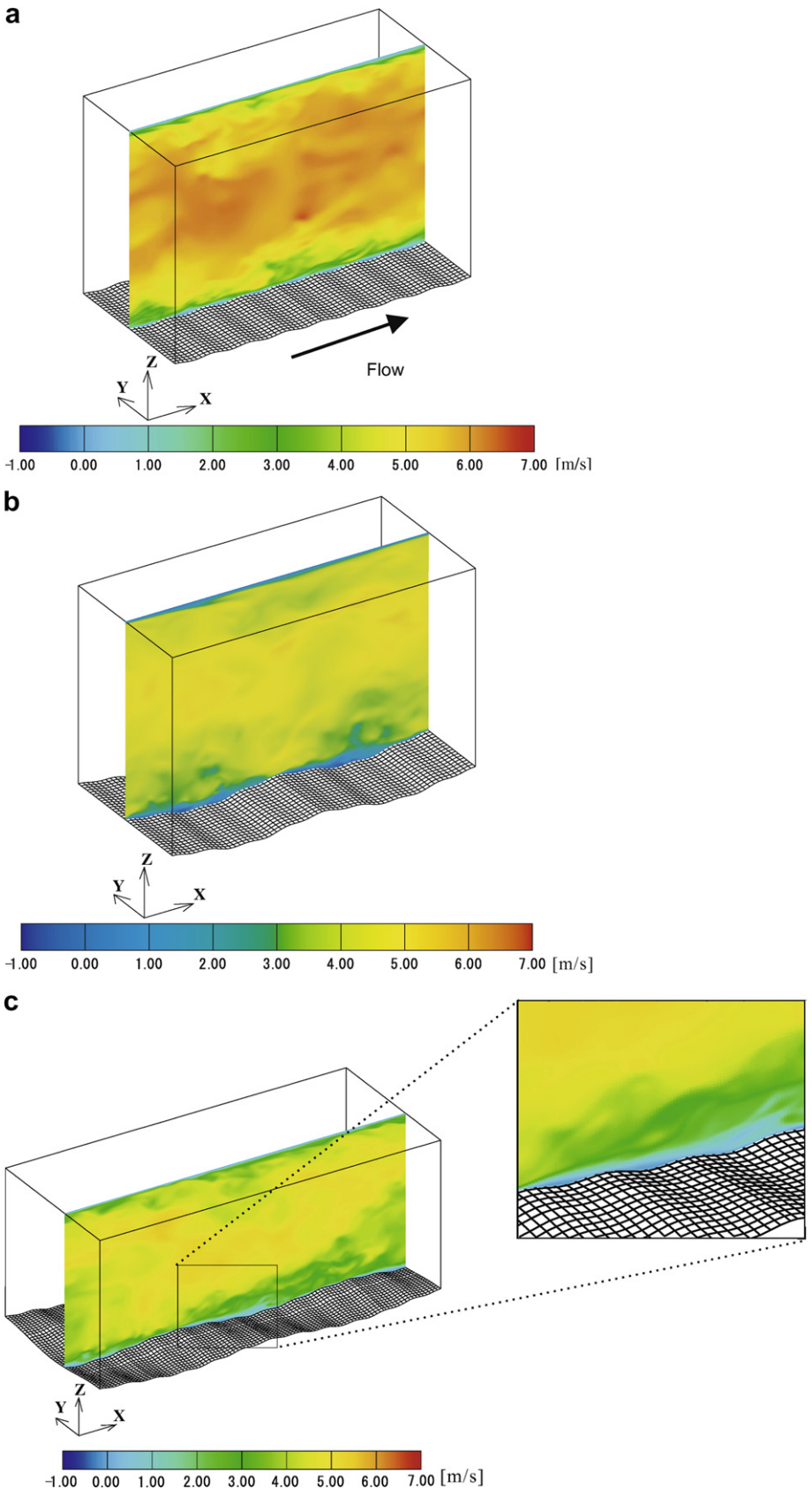

Fig. 2. Distributions of instantaneous streamwise velocity on the x–z plane: (a) case 1: pure wind wave; (b) case 2: parallel-swell wind wave (0° oblique-swell); (c) case 4: 48° oblique-swell wind wave.

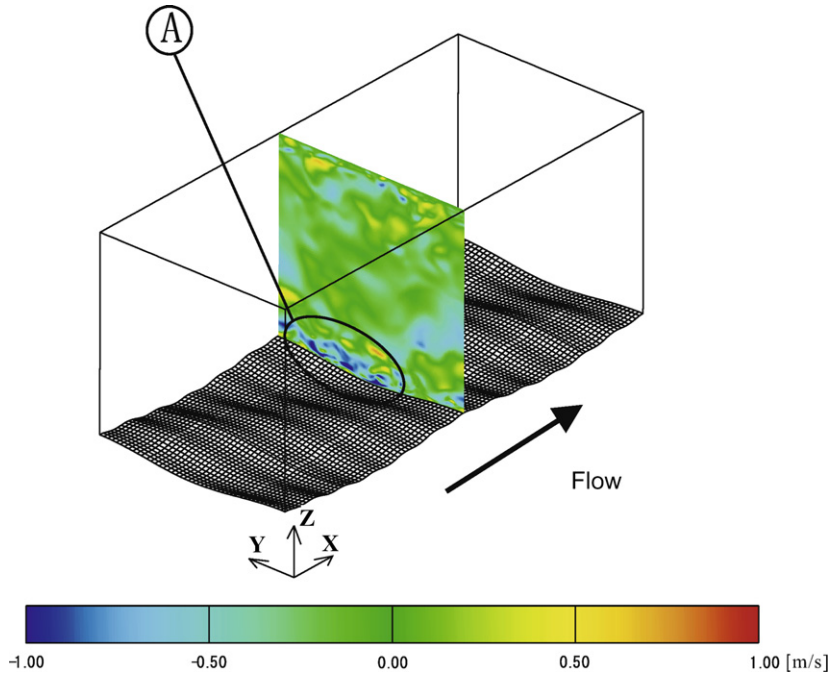

Fig. 3. Distribution of instantaneous spanwise velocity on the y–z plane in case 4.

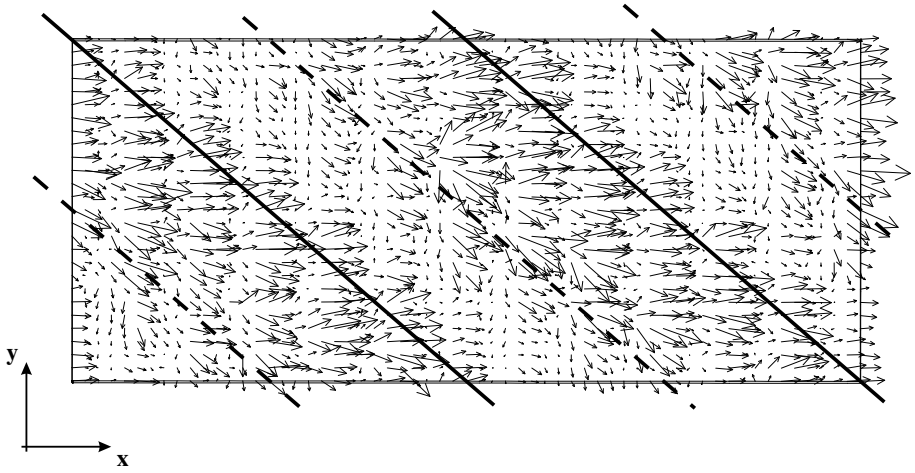

Fig. 4. Instantaneous velocity vectors near the wavy wall on the grid correlated plane in case 4. Solid lines denote the crest of swell and dashed lines denote the trough of swell. (Distance from wavy wall, $z' = 1.4 \times 10^{-3}$.)

$$D_{\mathrm{p}} = -\frac{1}{A}\int\int_{S} p_w e_{\mathrm{n}} \cdot e_x \,\mathrm{d}S, \tag{3}$$

$$D_{\mathrm{f}} = -\frac{1}{A}\int\int_{S} \tau_{\mathrm{w}} e_t \cdot e_x \,\mathrm{d}S, \tag{4}$$

where p_{w} and τ_{w} denote the local mean pressure and local mean streamwise shear stress, respectively. The vectors e_{n}, e_{l} and e_x are the wall normal unit vector, wall tangential unit vector and streamwise unit vector, respectively, and A denotes the vertical projected area of the walls. Since the present flows are kinds of channel flow, friction drag on the upper flat wall, $D_{\mathrm{F,f}}$ exists besides pressure and friction drags on the lower wavy walls, $D_{\mathrm{P,w}}$ and $D_{\mathrm{F,w}}$. The ratios of these drags to the total drag, D_{T} ($=D_{\mathrm{F,f}} + D_{\mathrm{P,w}} + D_{\mathrm{F,w}}$.), are shown in Fig. 9 for all cases.

The comparison of case 1 with case 2 shows that the parallel swell increases $D_{\mathrm{P,w}}$, but it decreases $D_{\mathrm{F,w}}$. As a result, the parallel swell increases the total drag, $D_{\mathrm{T,w}}$ ($= D_{\mathrm{P,w}} + D_{\mathrm{F,w}}$), on the wavy wall because of the remarkable increase of $D_{\mathrm{P,w}}$. However, as the swell angle, θ, increases, the swell effects become small and finally almost vanish as in case 6 (perpendicular swell). Our previous mass transfer measurements in a wind wave tank showed that swell decreases the mass transfer velocity across the wavy air–water interface, but the physical reason has not been fully clarified. Considering that the mass transfer velocity is strongly affected by turbulent motions (surface-renewal eddies) generated

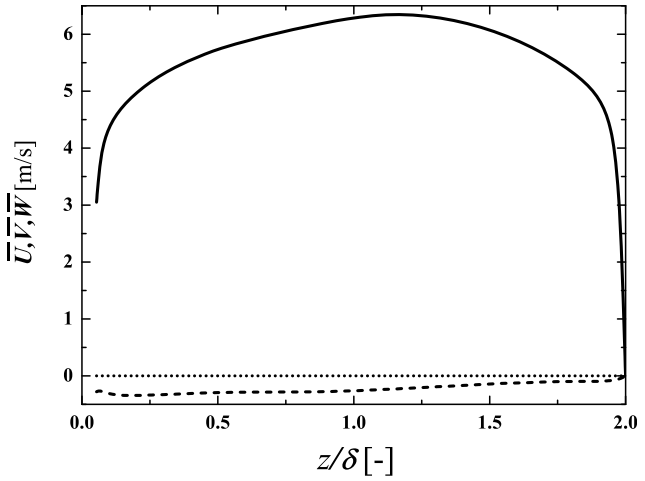

Fig. 5. Vertical distributions of mean velocities in case 4; (—), $\overline{U}$; (---), $\overline{V}$; (···), $\overline{W}$.

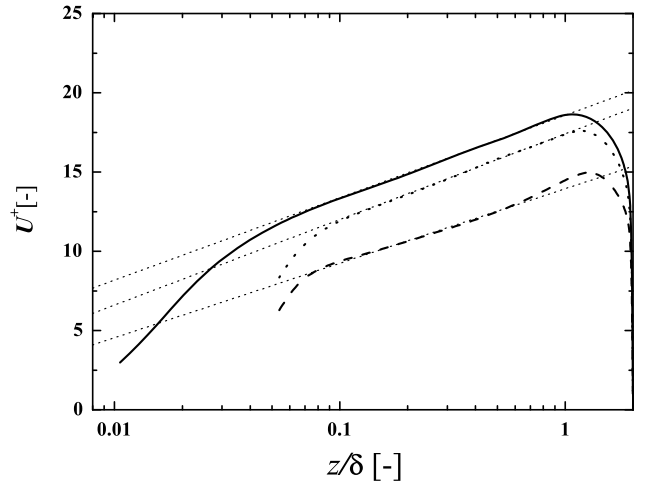

Fig. 6. Vertical distributions of mean streamwise velocity: (—), pure wind wave (case 1); (---), parallel-swell wind wave (case 2); ···, 48° oblique-swell wind wave (case 4).

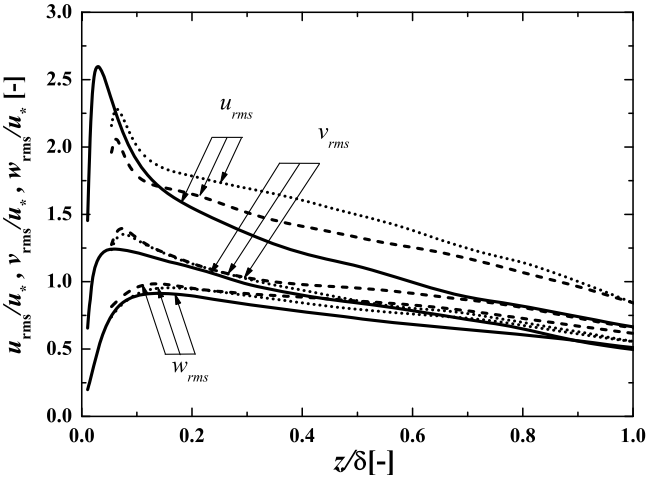

Fig. 7. Vertical distributions of turbulence intensities. Lines are as in Fig. 6.

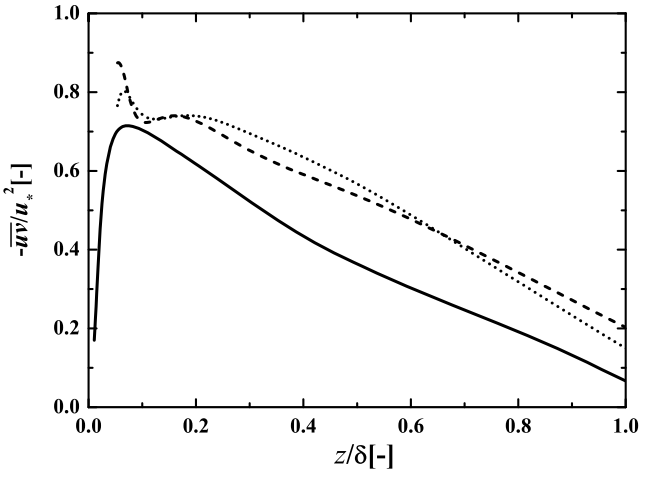

Fig. 8. Vertical distributions of the Reynolds stress. Lines are as in Fig. 6.

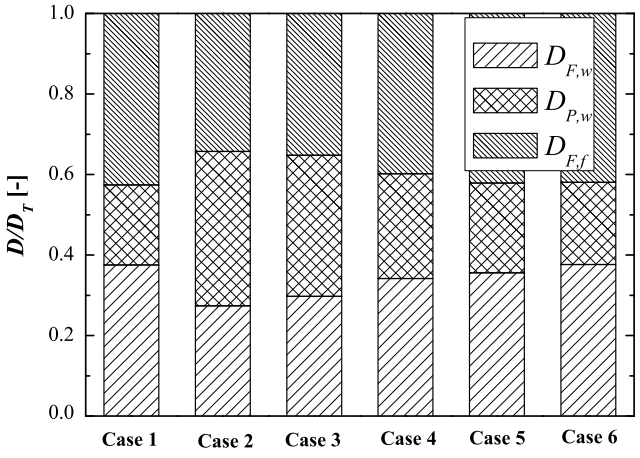

Fig. 9. Contributions of pressure and friction drags to the total drag.

beneath the interface by the friction drag, the present results suggest that reduction of mass transfer velocity due to swell is caused by decrease of friction drag on the wind-driven wavy air–water interface. Furthermore, the reduction effect is expected to be weakened by increase of swell angle and finally vanishes for the perpendicular swell (case 6).

Fig. 10 shows the relation between the swell angle, θ, and the friction drag on the wavy walls. It is found that $D_{\mathrm{F,w}}$ increases almost linearly with θ. The approximate expression is given as

$$D_{\mathrm{F,w}}(\theta)/D_{\mathrm{T}} = 0.068\theta + 0.27 \quad (0 \leqslant \theta \leqslant \pi/2), \tag{5}$$

and can also be written as

$$D_{\mathrm{F,w}}(\theta) = D_{\mathrm{F,case\,2}}(1 + 0.25\theta) \quad (0 \leqslant \theta \leqslant \pi/2), \tag{6}$$

by using the friction drag on the parallel-swell wind wave (case 2), $D_{\mathrm{F,\,case\,2}}$. This suggests that the friction drag acting on the wind-driven air–water interface, consisting of an arbitrary-angle swell and wind wave, can be estimated from the friction drag on the parallel-swell wind wave; and the

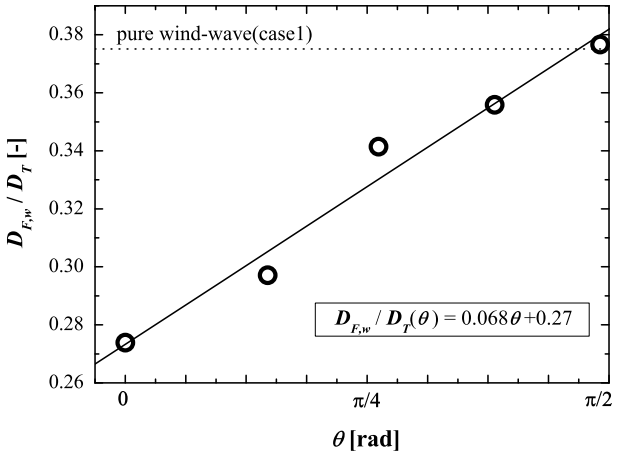

Fig. 10. Relation between swell angle and friction drag.

mass transfer velocity can also be estimated from measurement of the mass transfer velocity for a parallel-swell wind wave.

3.3. Local pressure and shear stress on wavy walls

In order to elucidate the reason why the pressure drag is increased and the friction drag is reduced by the swell, local pressures and shear stresses on wavy walls were examined. Figs. 11 and 12 show the streamwise distributions of the mean pressure on wavy walls in cases 1, 2 and 4. In these figures, the shapes of wavy walls in cases 2 and 4 are also illustrated. It is found that the pressure in all cases tend to be high at the trough of a wind wave and low at the crest, although the trend is gentle on the windward side of the swell. The pressure is also higher in cases 2 and 4 than in case 1 in the trough of swell, especially on the leeward side of the trough. This is because the wavy wall blocks the stream on the leeward side of the trough. However, the rate of increase of pressure in case 4 is smaller than in case 2, since the shape of the wavy wall in the streamwise direction is blunter in case 4 than in case 2. The results agree with the contribution of pressure drag shown in Fig. 9.

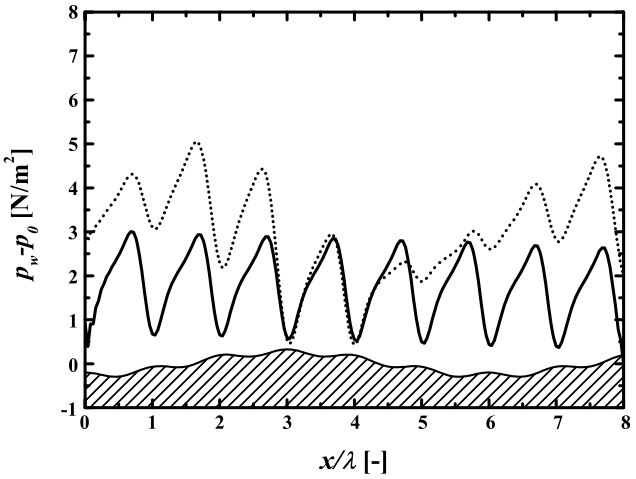

Fig. 12. Streamwise distributions of pressure on wavy walls: (—), pure wind wave (case 1); (···), 48° oblique-swell wind wave (case 4).

On the other hand, the streamwise distributions of the mean streamwise shear stress on the wavy walls are shown in Figs. 13 and 14. In these figures, the shapes of wavy walls in cases 2 and 4 are also illustrated. It is observed that the streamwise shear stress in all cases is high on the windward side of the wind wave's crest and low on the leeward side. The streamwise shear stress is higher in cases 2 and 4 than in case 1 on the windward side of the swell crest, but lower on the leeward side. The effects on the streamwise shear stress are weaker in case 4 than in case 2 because of the bluntness of the oblique swell. Comparing the amounts of increase and decrease of shear stress by swell, the decrease is stronger than the increase. The results are consistent with the swell effects on friction drag shown in Fig. 9.

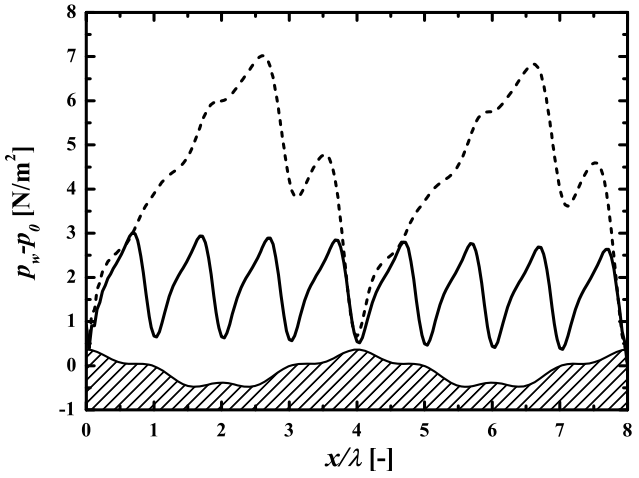

Fig. 11. Streamwise distributions of pressure on wavy walls: (—), pure wind wave (case 1); (---), parallel-swell wind wave (case 2).

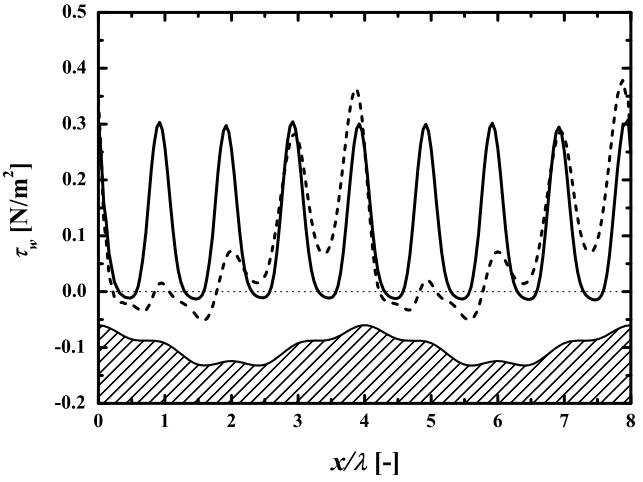

Fig. 13. Streamwise distributions of shear stress on wavy walls. Lines are as in Fig. 11.

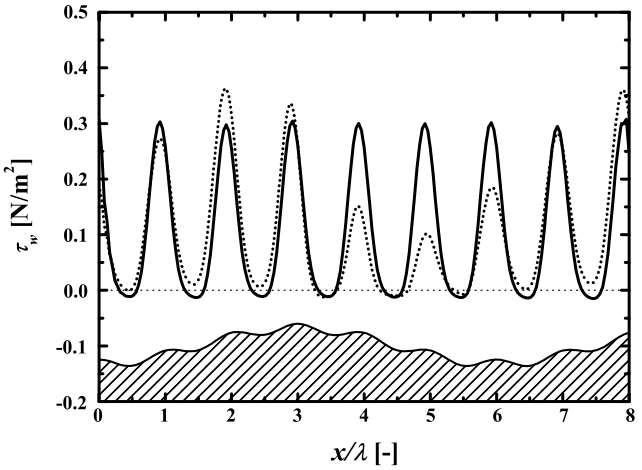

Fig. 14. Streamwise distributions of shear stress on wavy walls. Lines are as in Fig. 12.

4. Conclusions

In our previous mass transfer measurements in a wind wave tank, swell was found to reduce the mass transfer velocity across the wind-driven air–water interface (Tanno and Komori, 2004) for a case where the phase velocities of the swell and wind wave are slower than the wind velocity. To elucidate the mechanism, three-dimensional direct numerical simulations (DNS) were here applied to the turbulent boundary layer over a wavy wall, which imitates the air–water interfaces consisting of both wind wave and swell with an arbitrary angle to the wind direction. From the numerical predictions by the DNS, turbulence structure and drag over/on the wavy walls were investigated in detail.

The results show that parallel swell increases the turbulence intensities and the Reynolds stress over the wavy walls. The swell also increases the pressure drag and decreases the friction drag on the wavy wall, and consequently increases the total drag because of the remarkable increase of the pressure drag. The reduction of the friction drag due to the swell suggests that the reduction of mass transfer velocity observed in our previous experiments is caused by suppression of wind-driven turbulence (surface-renewal eddies) beneath the air–water interface by swell, since the surface-renewal turbulent motions produced by the friction drag control the mass transfer across the air–water interface.

The effects of oblique swells on the turbulence structure and drag over/on wavy walls have not been previously examined by experiments. The results show that the effects of the swell on the drag become weak and finally vanish with increase of inclination angle of the swell from parallel to perpendicular. The friction drag is linearly correlated with the inclination angle of the swell. These mean that the reduction effect on the mass transfer across the air–water interface due to the swell is suppressed by the obliqueness of the swell and that the reduction rate can be roughly estimated by the inclination angle. This finding can be useful in estimating precisely the CO_2 transfer rate across the air–sea interface.

Acknowledgement

This research was supported by a Ministry of Education, Science, Sports and Culture Grant-in-Aid (No. 19206023). The authors are grateful to Dr. K. Nagata, Nagoya University, for many useful discussions. They also thank T. Yamamoto for his help in conducting numerical simulations.

References

Angelis, V.D., Lombardi, P., Banerjee, S., 1997. Direct numerical simulation of turbulent flow over a wavy wall. Phys. Fluids A 9, 2429–2442.

Belcher, S.E., Hunt, J.C.R., 1998. Turbulent flow over hills and waves. Annu. Rev. Fluid Mech. 30, 507–538.

Fulgosi, M., Lakehal, D., Banerjee, S., De Angelis, V., 2003. Direct numerical simulation of turbulence in a sheared air–water flow with a deformable interface. J. Fluid Mech. 482, 319–345.

Günther, A., von Rohr, P.R., 2003. Large-scale structures in a developed flow over a wavy wall. J. Fluid Mech. 478, 257–285.

Hudson, J.D., Dykhno, L., Hanratty, T.J., 1996. Turbulence production in flow over a wavy wall. Exp. Fluids 20, 257–265.

Komori, S., 1996. Turbulence structure and CO_2 transfer at the air–sea interface and turbulent diffusion in thermally-stratified flows. CGER's Supercompute Monograph Report 1.

Komori, S., Murakami, Y., Ueda, H., 1989. The relationship between surface-renewal and bursting motions in an open-channel flow. J. Fluid Mech. 203, 103–123.

Komori, S., Nagaosa, R., Murakami, Y., 1993a. Turbulence structure and mass transfer across a sheared air–water interface in wind-driven turbulence. J. Fluid Mech. 249, 161–183.

Komori, S., Nagaosa, R., Murakami, Y., Chiba, S., Ishii, K., Kuwahara, K., 1993b. Direct numerical simulation of three-dimensional open-channel flow with zero-shear gas–liquid interface. Phys. Fluids A 5, 115–125.

Krettenauer, K., Schumann, U., 1992. Numerical-simulation of turbulent convection over wavy terrain. J. Fluid Mech. 237, 261–299.

Lakehal, D., Fulgosi, M., Banerjee, S., 2003. Direct numerical simulation of turbulent heat transfer across a mobile, sheared gas–liquid interface. ASME J. Heat Transfer 125, 1129–1139.

Magnaudet, J., Calmet, I., 2006. Turbulent mass transfer through a flat shear-free surface. J. Fluid Mech. 553, 155–185.

Nakagawa, S., Hanratty, T.J., 2001. Particle image velocimetry measurements of flow over a wavy wall. Phys. Fluids 13, 3504–3507.

Nakayama, A., Sakio, K., 2003. Direct numerical simulation of turbulent flow over complex wavy rough surface. J. Appl. Mech., JSCE 6, 839–846 (in Japanese).

Sullivan, P.P., McWilliams, J.C., 2002. Turbulent flow over water waves in the presence of stratification. Phys. Fluids 14, 1182–1195.

Sullivan, P.P., McWilliams, J.C., Moeng, C., 2000. Simulation of turbulent flow over idealized water waves. J. Fluid Mech. 404, 47–85.

Poggi, D., Porporato, A., Ridolfi, L., 2003. Analysis of the small-scale structure of turbulence on smooth and rough walls. Phys. Fluids 15, 35–46.

Tanno, K., Komori, S., 2004. Effects of swell turbulence structure and mass transfer across the wind-driven air–water interface. Trans. JSME. Ser. B., 644–649 (in Japanese).

Wanninkhof, R., 1992. Relationship between wind speed and gas exchange over the ocean. J. Geophys. Res. 97, 7373–7382.

Zilker, D.P., Cook, G.W., Hanratty, T.J., 1977. Influence of the amplitude of a solid wavy wall on a turbulent flow. Part 1. Non-separated flows. J. Fluid Mech. 82, 29–51.